GEOPHYSICS, VOL. 71, NO. 3 (MAY-JUNE 2006); P. V79–V86, 9 FIGS.
10.1190/1.2196875

Application of complex-trace analysis to seismic data for random-noise suppression and temporal resolution improvement

Hakan Karsli[1], Derman Dondurur[2], and Günay Çifçi[2]

ABSTRACT

Time-dependent amplitude and phase information of stacked seismic data are processed independently using complex trace analysis in order to facilitate interpretation by improving resolution and decreasing random noise. We represent seismic traces using their envelopes and instantaneous phases obtained by the Hilbert transform. The proposed method reduces the amplitudes of the low-frequency components of the envelope, while preserving the phase information. Several tests are performed in order to investigate the behavior of the present method for resolution improvement and noise suppression. Applications on both 1D and 2D synthetic data show that the method is capable of reducing the amplitudes and temporal widths of the side lobes of the input wavelets, and hence, the spectral bandwidth of the input seismic data is enhanced, resulting in an improvement in the signal-to-noise ratio. The bright-spot anomalies observed on the stacked sections become clearer because the output seismic traces have a simplified appearance allowing an easier data interpretation. We recommend applying this simple signal processing for signal enhancement prior to interpretation, especially for single channel and low-fold seismic data.

INTRODUCTION

Seismic data with high temporal and spatial resolution, as well as low coherent and random noise content, are clearly easier to interpret. Many seismic data-processing techniques have been developed to address resolution and noise issues and improve the quality of seismic stacks and images (Klemperer, 1987; Yilmaz, 1987; Gülünay, 2000; Ristau and Moon, 2001). In general, processing techniques are most efficient for high fold data.

We assume that preprocessing has been done to optimally improve resolution and S/N ratio on the sections to be interpreted. We note that in complex geologic structures, the seismic data may still have a complex character because of interference effects (Felsen and Markuvitz, 1973; Gelchinsky and Karaev, 1980). Seismic-data displays of phase and group characteristics are useful for interpretation (Farnbach, 1975; Gelchinsky et al., 1985). The phase and group characteristics can be determined by representing the seismic trace as the real part of a complex function of time. This procedure, known as complex-trace analysis, has been used successfully for the interpretation of stacked seismic sections, especially by means of instantaneous amplitude, phase and frequency sections (Taner et al., 1979; Gelchinsky et al., 1985; Shtivelman et al., 1986). Although complex-trace analysis is a common tool in seismic interpretation, its applications are generally restricted to the extraction of instantaneous attribute information from seismic data (Morozov and Smithson, 1996), especially for the regions where large-scale bright spots occur (e.g. Yilmaz, 1987). Shtivelman et al. (1986), however, have used this method for wavefield analysis in complex heterogeneous media producing normalized phase and group trace sections. They pointed out that these two types of sections represent different features of wavefields and can differ considerably. The group section denotes the place of energy concentration on sections and gives a general definition of the subsurface, whereas the phase section represents the zones of continuous-phase correlation and gives more details of the subsurface structure. Their combined analysis can help in building a more reliable, complete seismic model of the subsurface.

We propose a procedure, complex-trace transformation (CTT) that uses complex-trace envelope and normalized phase traces to improve the temporal resolution and to increase S/N of stacked seismic data. We follow the technique offered by Shtivelman et al. (1986), who showed that analysis of seismic data in complex geologic environments should be based on both group and phase correlation.

In this study, we suggest further applications of the method for

Manuscript received by the Editor February 23, 2004; revised manuscript received November 18, 2005; published online May 24, 2006.
[1]Karadeniz Technical University, Department of Geophysics, 61080 Trabzon, Turkey. E-mail: hkarsli@ktu.edu.tr.
[2]Dokuz Eylül University, Institute of Marine Sciences and Technology, Bakü Street, No. 32, 35340, Inciraltı, İzmir, Turkey. E-mail: dermon.dondurur@deu.edu.tr; gunay.cifci@deu.edu.tr.

resolution improvement and random-noise suppression, which have not been considered by Shtivelman et al. (1986). The applicability of the method for temporal resolution improvement in presence of interference effects and random noise is also discussed with examples of synthetic and field seismic data. Several tests are performed on both 1D and 2D models. The results from an *f-x* prediction filter and a K-L transform are presented for comparing the efficiency of the CTT method.

CTT METHOD

Using amplitude and phase information, seismic traces can be expressed as

$$S(t) = R(t)\cos\theta(t), \tag{1}$$

where $R(t)$ is the envelope and $\theta(t)$ is the time-dependent phase information of the seismic trace, both of which can be determined from the seismic-trace $S(t)$ by Hilbert transform. Rewriting equation 1 to obtain the envelope and normalized phase of the trace, we obtain

$$S(t) = R(t)\cos\theta_n(t), \tag{2}$$

where $\theta_n(t)$ is normalized phase or the cosine of the instantaneous phase $\theta(t)$ and can be expressed as

$$\theta_n(t) = S(t)/R(t). \tag{3}$$

Decomposition of seismic traces into amplitude and phase traces causes no information loss because the actual seismic trace can be reconstructed by linear multiplication of $R(t)$ and $\theta_n(t)$, according to equation 2.

The envelope is a positive-valued trace; however, one can convert the envelope trace to an oscillating time series with both positive and negative values similar to the input seismic trace. To do this, the low-frequency component $b(t)$ is computed, for instance as a running average within a given-time window, T_w, and subtracted from $R(t)$,

$$g(t) = R(t) - b(t). \tag{4}$$

The result of the reconstruction is the so-called group trace (Shtivelman et al., 1986; Karsli, 2002). Determination of the time window length (T_w) is important, and its influence on the output data will be discussed later. After several tests and applications in this study, we have achieved satisfactory results with the following criterion for the selection of T_w:

$$(N/8)\Delta t \le T_w \le (N/4)\Delta t, \tag{5}$$

where N is the number of data samples per trace and Δt is time sampling interval.

Seismic traces can be decomposed into their normalized-phase and group-trace components and can then be reconstructed to compare with the input seismic trace as follows (Shtivelman et al., 1986):

$$h(t) = g(t)\,\theta_n(t), \text{ for } g(t) \le 0; \tag{6}$$

$$h(t) = 0, \text{ for } g(t) \le 0. \tag{7}$$

Equations 6 and 7 express the reconstruction of the final seismic traces using their normalized phase and group traces.

Here, we propose that the zero and negative parts of the group traces correspond to side lobes and low-frequency random-noise components of the seismic data, because the group trace is obtained by subtracting the low-frequency component from the envelope trace. Therefore, the omission of zero or negative values in the group trace can improve the temporal resolution and decrease the low-frequency random-noise level in the seismic data.

RESULTS

For the application of the method, it is important to determine what is removed by the algorithm and what is left on the seismograms. Basically, the main characteristic of the CTT method is that the amplitude of the signal component in the trace is simply reduced when the amplitude of the signal (mainly side lobes) is close to that of the low-frequency component of the envelope; therefore low-frequency or low-amplitude noise is reduced while strong reflections and high-frequency events such as spikes are preserved. This process also improves the temporal resolution because the amplitudes of the side lobes are reduced.

Tutorial examples with 1D signals

We applied the method to a series of Ricker wavelets with a constant dominant frequency of 40 Hz (Figure 1). We used different peak amplitudes ranging from 1 to −1 (Figure 1a) in order to investigate how the method affects the different amplitude values on a trace without taking into consideration the frequency content. Figure 1b and c show the envelope of the signal and the running average (or low-frequency component) of the envelope, respectively. Because the frequency content of the input signal is constant, the low-frequency component has relatively low-amplitude values. The group and signal estimate traces are shown in Figures 1d and 1e, respectively. Note that phase and polarity characteristics of the input signal are not disturbed in the output. The differences between input (Figure 1a) and output (Figure 1e) signal amplitudes are illustrated in Figure 1f. The amplitude reductions in the filtered trace appear to be small with respect to the strongest-signal components of the input trace. Also, the amplitude reductions are relatively insensitive to the amplitudes of the input-signal components.

In order to illustrate the performance of the method as a function of the frequency content of the input signal, we apply the CTT to a number of Ricker wavelet with different frequencies ranging from 5 to 100 Hz (Figure 2a) with 5 Hz increments. The peak amplitudes of these Ricker wavelets are chosen as unity in order to see how the method affects the amplitudes of the wavelets with different dominant frequencies. The low-frequency component (Figure 2c) has greater values for low-frequency (5 to 15 Hz) Ricker wavelets between 0 and 1 s, as expected. The group and output signals are shown in Figure 2d and e, respectively. In order to show the amplitude reductions of each individual Ricker wavelet, the differences between input (Figure 2a) and output (Figure 2e) signal amplitudes are illustrated in Figure 2f. It is observed from Figure 2e and f that most of the amplitude reduction in the signal occurs in

the low-frequency wavelets between 0 and 15 Hz bandwidth, while the method seems to have relatively insignificant effect on the amplitudes of the wavelets with dominant frequencies greater than 20 Hz. This is because the algorithm attempts to reduce the signal amplitude whose frequency is close to the running average of the envelope multiplied by its normalized phase. This frequency bandwidth can be changed by adjusting the time window of the running-average operator, T_w.

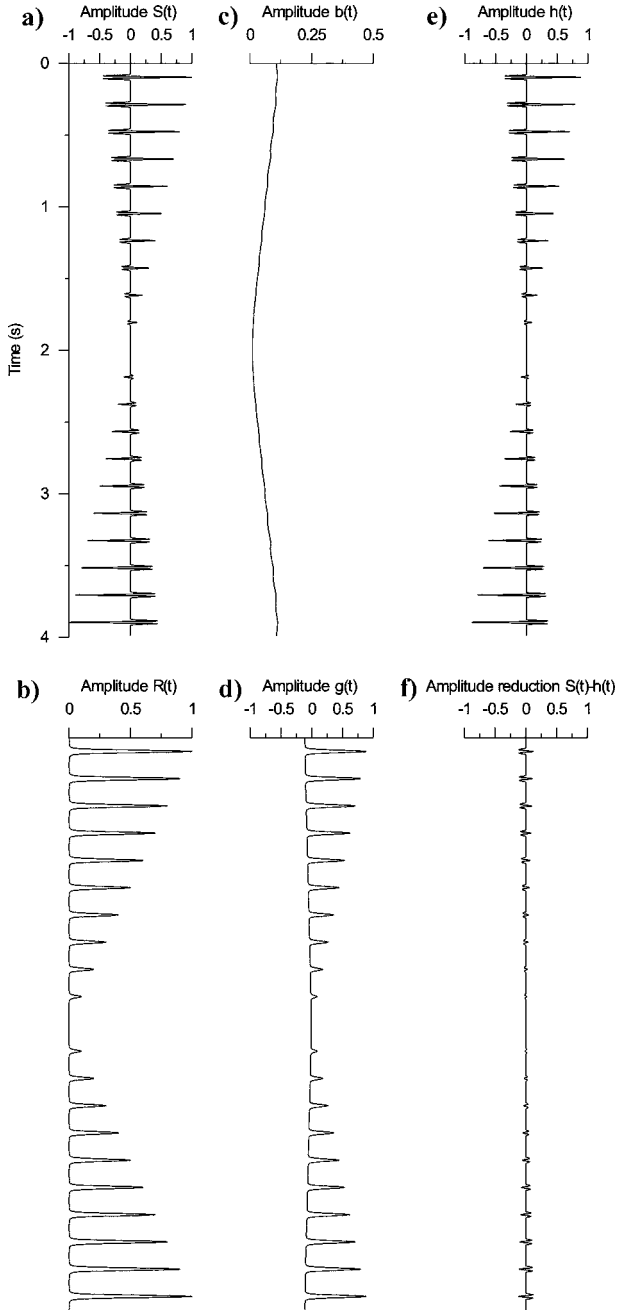

Figure 1. Efficiency test of the method on amplitude values of the input signal. (a) Input signal composed of several constant-frequency (40-Hz) Ricker wavelets with different amplitudes ranging between 1 and −1, (b) envelope of the input signal, (c) low-frequency component of the signal envelope, (d) group signal, (e) output signal and (f) amplitude differences between input (a) and output (e) signals. Note that the amplitude reduction is almost constant through the signal when the frequency content of the input signal is constant.

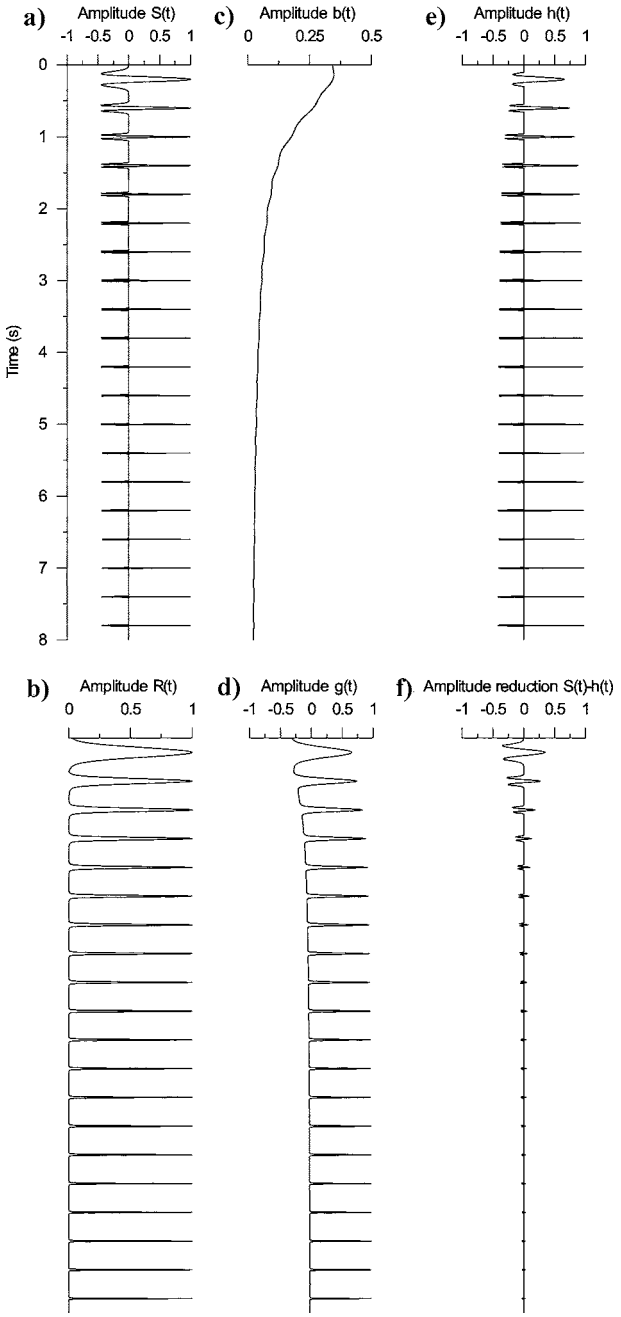

Figure 2. Efficiency test of the method on frequency content of the input signal. (a) Input signal composed of several unit-amplitude Ricker wavelets with different dominant frequencies varying from 5 to 100 Hz with 5-Hz increment, (b) envelope of the input signal, (c) low-frequency component of the signal envelope, (d) group signal, (e), output signal and (f) amplitude differences between input (a) and output (e) signals. Note that most of the amplitude reduction in the output occurs in the low-frequency wavelets between 0- and 15-Hz interval.

Effect of time window length T_w

In order to evaluate the effect of time window length on the output data, the CTT method is applied to a 20-Hz Ricker wavelet with 10% white noise using a number of different time window lengths. The input wavelet and its amplitude envelope are shown in Figure 3a. Figure 3b shows the low-frequency component of the envelope computed from equation 4 using different T_w values, while Figure 3c shows outputs of the CTT method for different T_w values. The maximum value of the low-frequency component approaches the maximum value of the amplitude envelope when the time window length is short (Figure 3b), which results in relatively high-amplitude reduction in the main lobe of the output wavelet (Figure 3c). Thus, a small time window length does not contribute to random-noise suppression, which is especially evident at the amplitudes where no amplitude is present except noise (e.g., between the times −0.1 and −0.05 s, and between 0.1 and 0.05 s in Figure 3c). Additionally, because the main-lobe amplitude of the wavelet in the output is quite small for small T_w values, random noise clearly dominates the main-lobe amplitude (see output trace for $T_w = (N/20)\Delta t$ around 0 s in Figure 3c).

Figure 3d illustrates the amplitude reductions after application of the CTT algorithm for noise-free input test signals with different central frequencies. The amplitude reduction is much larger at lower frequencies for all T_w values, and it decreases as the center frequency of the input wavelet increases (Figure 3d). It is also evident that T_w controls the frequency content of the CTT output. For instance, the amplitude reduction is very low and almost constant for frequencies higher than 30 Hz when $T_w = (N/2)\Delta t$. The amplitude reduction, however, is relatively high ($>50\%$) for all frequencies when $T_w = (N/40)\Delta t$.

Although amplitude reduction always occurs in the output because of the nature of the CTT algorithm, its amount is controlled by T_w. In Figure 4, we illustrate numerically the trade-offs between improving temporal resolution and signal preservation as a function of the parameter T_w. According to Figure 4b, the amplitude ration between main lobe and side lobe is maximum between $T_w = (N/8)\ t$ and $T_w = (N/4)\Delta t$, which states that there is a trade-off between side-lobes reduction (high for small T_w) and main-lobe preservation (good for large T_w). At the same time, the temporal width of the output wavelet is also minimal within this T_w range. Therefore, we conclude that the T_w should be chosen between $(N/8)\Delta t$ and $(N/4)\ t$ in order to simultaneously take both advantages of the method: temporal resolution improvement and random-noise suppression.

Examples of improved temporal resolution

Two reflections from top and bottom of a thin layer are resolved temporally when they are seen as separate reflection events, and this is generally governed by the thickness of the layer, its velocity, and the dominant frequency of the data. If the interference of the reflections and the effects of their side lobes can be reduced, the frequency content of stacked seismic data is enhanced while vertical (temporal) resolution improves.

The side lobe reduction of the CTT algorithm is presented in Figure 3c on a simple Ricker wavelet. In order to investigate the performance of the method on a seismic section, we produce a 2D depth model of a marine environment consisting of curved interfaces that simulates bedded sediments with two onlap terminations against a basin-formed (low-angle) interface (Figure 5a). A synthetic time section of the depth model is produced using normal incidence ray tracing (exploding reflectors) to simulate the unmigrated-stack section (Figure 5b). A zero-phase 20 Hz Ricker wavelet is used to compute the time section sampled at 1 ms with 5-m trace interval. The computation of the synthetic seismograms in-

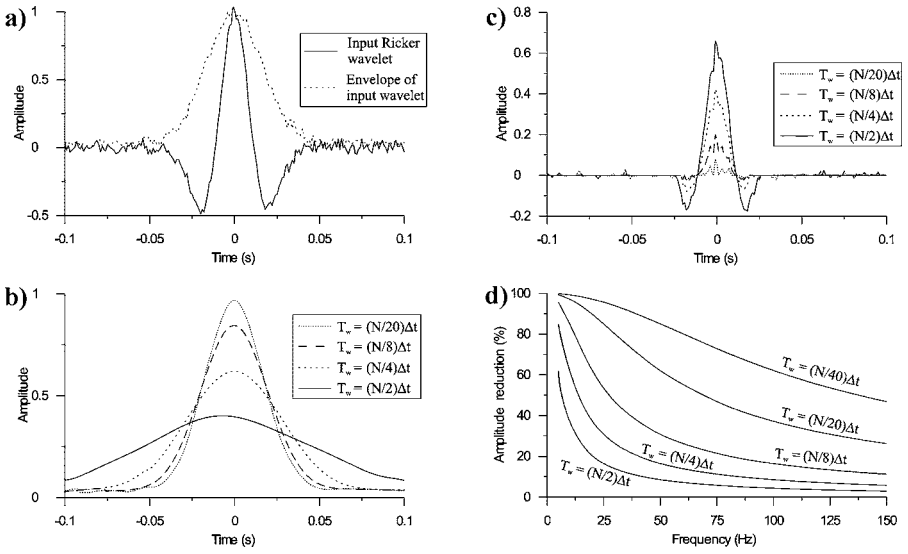

Figure 3. Application of the CTT method to test the effect of time window length T_w. (a) Input 20-Hz Ricker wavelet with 10% random noise and its amplitude envelope, (b) low-frequency components of the envelope computed using different T_w values, (c) output wavelets for different T_w values, and (d) effect of T_w value on the amplitude reduction versus frequency content of the input.

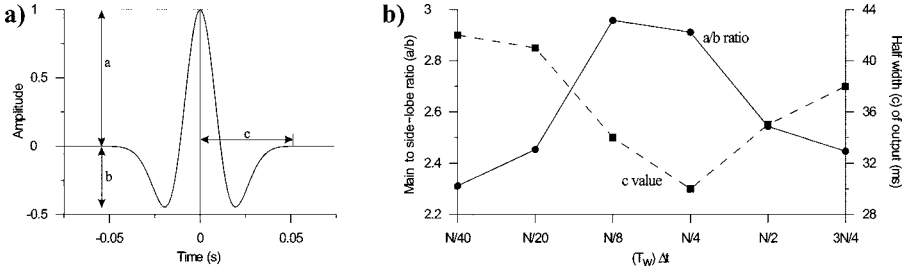

Figure 4. The effect of the method both in amplitude and temporal width of the input. (a) Input 20-Hz Ricker wavelet without noise and its parameters, a: main-lobe amplitude, b: side-lobe amplitude, and c: half-time width; (b) Trade-off between main- to side-lobe amplitude ratio (a/b) and the change in the half-width of the output for different T_w values.

volves primary P-wave reflections without random and coherent noise such as S-waves, multiples and diffractions. The synthetic data are then corrected for spherical divergence. Figure 5c shows the output seismograms obtained by an application of the CTT method to the synthetic section in Figure 5b. Two close-ups show the detailed image of two onlap terminations (A and B) located at about 0.25 and 0.36 s. While the two reflections from top and bottom interfaces can be separated completely by trace 66 for termination A, and trace 87 for termination B in the input section, it is possible to identify both interfaces towards the traces 71 and 92, respectively, in the output seismograms. When comparing input and output close-ups, this effect can also be observed in the reflection-free area between two onlap terminations. On the other hand, it should be noted that the method also produces small-scale changes in the character and frequency of the interference pattern, which is especially evident in the waveform of the bottom-reflection event of onlap B in the close-up of output seismograms (Figure 5c).

Examples of random-noise suppression

The applicability of the method for random-noise suppression is illustrated in Figure 6 using a 1D earth model consisting of constant-density layers (Figure 6a). The synthetic seismic trace obtained from convolving a 20-Hz Ricker wavelet with the reflection coefficients obtained from the depth model is produced (solid line in Figure 6b) together with random noise (dashed line in Figure 6b). Figure 6c shows the spectral characteristics of both signal (solid line) and noise traces (dashed line). The spectrum bandwidth of the signal changes between 0 and 160 Hz, while the random noise spectral bandwidth has a whiter spectrum and the frequency spectra of both signal and noise series overlap between 0- and 120-Hz frequency band. After summing the signal and noise traces, we obtain the noisy seismic trace shown in Figure 6d, which is used as an input to the CTT algorithm. The output trace obtained from the method application is shown in Figure 6e. Because the method attempts to reduce the amplitudes of low-frequency components of the trace, the spectral characteristics (and hence the frequency content or spectral bandwidth) of both signal and noise are not considered separately. Although some residual noise components indicated by arrows exist in the output trace, we conclude that individual reflection events seen in the noise-free synthetic trace are preserved at their correct arrival times together with their correct phase and polarity characteristics in the output trace, while most of the random-noise components are attenuated. The amplitudes and

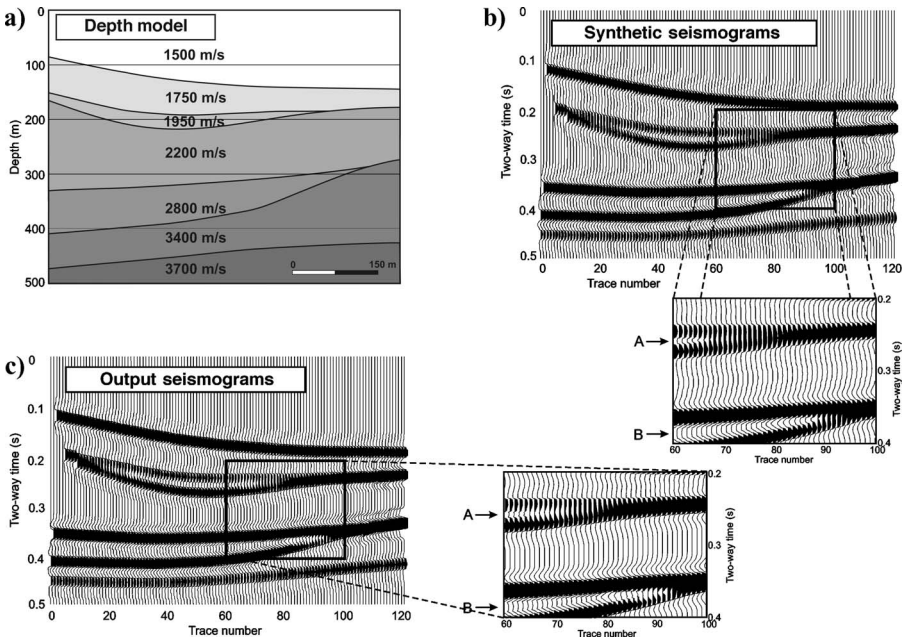

Figure 5. Investigation of the effectiveness of the method for resolution improvement on a 2D earth model. (a) 2D depth model consisted of several bedded-sedimentary layers with two onlap terminations; (b) noise-free synthetic section computed using normal-incidence ray-tracing with a 20-Hz Ricker wavelet, sampled at 1-ms and 5-m trace interval; (c) output seismograms obtained from the application of the method for T_w equal to 100 ms. Two closeups show the details of two onlap terminations (A and B) to compare the resolution between two successive reflections from both onlap terminations.

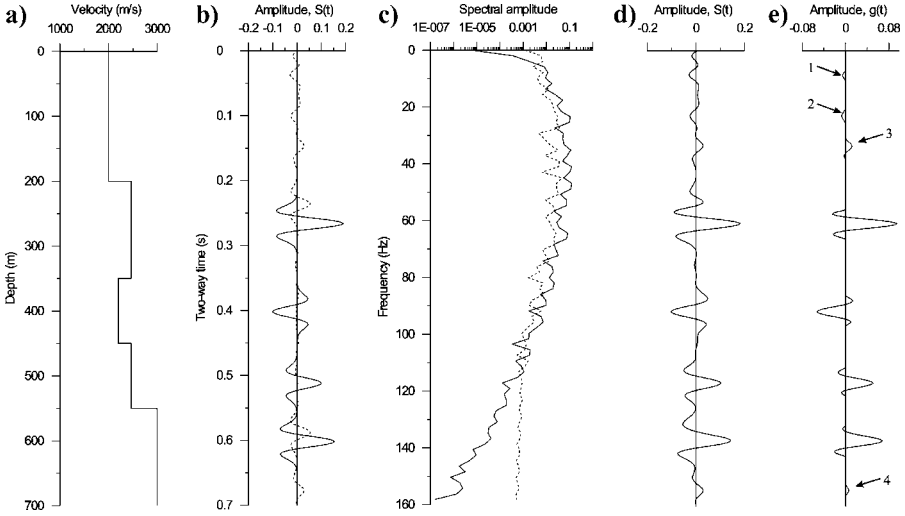

Figure 6. An application of the method for random-noise suppression. (a) 1D constant-density earth model, (b) the synthetic seismic trace (solid line) and relatively low-amplitude random noise (dashed line); (c) corresponding amplitude spectra of synthetic trace (solid line) and the noise trace (dashed line); (d) noisy trace obtained by summing signal and noise traces; (e) output trace obtained from application of the method to the noisy trace. Arrows indicate residual noise components in the output trace.

time widths of the side lobes in the input trace are reduced in the output.

In order to test further the applicability and the performance of the method on random-noise suppression, we applied 10% random noise to the synthetic seismograms in Figure 5b with 10% random noise addition (Figure 7a). For comparison, we also present the results of two well-known random-noise suppression processes, K-L and *f-x* prediction filters (Figure 7b and 7c, respectively). The number of eigenvectors used in the K-L filter is 21; the length of the prediction error operator and amount of prewhitening used in *f-x* filter is 21% and 10%, respectively. These parameters are determined by a trial-and-error method, and the optimal values are chosen after several tests. The methods and effects of optimal determination of these parameters will not be discussed here. However, the detailed explanations of these two filtering methods can be found in Hornbostel (1991) for *f-x* filter and in Hemon and Mace (1978) for K-L filter.

A window length T_w equal to 100 ms is used in the CTT application and the output seismograms from the CTT method is shown in Figure 7d. We observed that all three methods left some random-noise components in the output seismograms, especially at shallower parts of the sections (e.g., down to 0.15 s). The *f-x* and K-L filters produce a smooth output with respect to the CTT output, while CTT seems to be more successful in removing the residual noise between two onlapping events (e.g., between 0.25 and 0.35 s). We also observed that the essential features are preserved while the temporal resolution is improved in the CTT output (compare the onlap terminations in Figure 7b and 7c). Our experience showed that the performance of the CTT method in random-noise attenuation decreases as the noise level increases, and the *f-x* prediction filter produces more reliable results in such cases.

Note that when using CTT method in complex geologic environments with a relatively high random-noise level, output signal amplitude can also be reduced, and the continuity of the reflections is interrupted, especially in regions where significant fault shadow effects with relatively low-signal amplitudes exist. In such cases, the amplitudes of the weaker reflections are generally not consistent from one trace to another in the input seismograms. Therefore, the continuity of these weaker-reflection events with poor trace-by-trace consistency can be adversely affected during the subtraction process of the method defined by equation 4, which can cause discontinuities in the reflections. However, this inconvenience arises only in quite complex geologic environments and is partly important during picking of the reflections and can be problematic when using automatic event picking.

Real data examples

The CTT algorithm is applied to two marine seismic reflection sections, one of which is a single-channel seismic data from Sorokhin Trough, northern Black Sea region, where a number of diapiric uplifts accompanied by gas accumulations at both flanks occur (Çifçi et al., 2003). The other example is low fold marine seismic data from northern Gulf of Mexico (Hart et al., 1999).

The Sorokhin Trough seismic data were acquired during a Training-Through-Research-1996 (TTR-6) cruise using a single-channel recorder with a single 3-L air gun and a 75-m streamer with 6 active channels. The shot interval was 10 s (about 40 m), and the record length was 3 s at 1-ms sampling rate. The data were then corrected for spherical divergence, and predictive deconvolution with 350-ms operator length and 20-ms prediction time was applied. The Gulf of Mexico seismic data were acquired by the USGS Coastal and Marine Geology Team in 1998 using a 35-in^3 GI gun and a 240-m streamer with 24 active channels. The shot interval was 14 s (about 20–30 m), and the record length was 2 s at 0.25-ms sampling rate. The data were then resampled to 0.5 ms and a fourfold stack was applied after deconvolution and velocity analyses (Lee et al., 2001).

Figure 8 shows the application of the CTT method to the traces between 30 and 200 of seismic line (ps256) from Sorokhin Trough. The input section (Figure 8a) shows a number of parallel to subparallel and undisturbed sedimentary layers. Two high-amplitude bright-spot anomalies with polarity reversals because of the localized gas accumulations are indicated as strong reflections (SR). Figure 8b shows the result of the application of the algorithm for T_w equal to 450 ms. The main interfaces seen in the input section, and the bright-spot anomalies are well preserved in the output data, while the low-amplitude random noise, including noise observed clearly before the seabed reflection, is almost completely removed. As a consequence of the random-noise suppression, bright-spot anomalies become much clearer.

Figure 9a shows a part of a low fold Gulf of Mexico seismic line (gm98-11a) between traces 250 and 400. The line shows a number of parallel and undisturbed sedimentary layers with a strongly

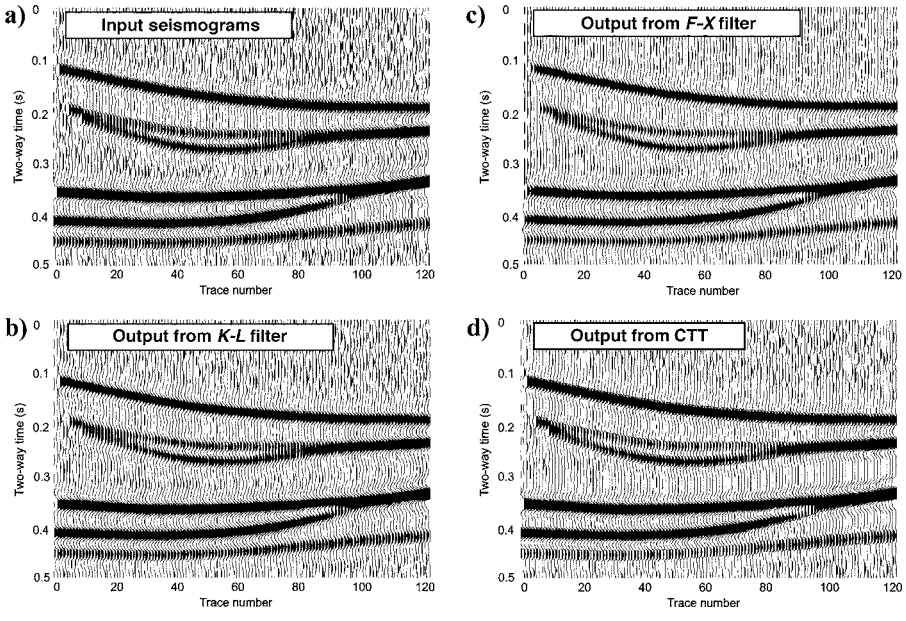

Figure 7. Investigation of the effectiveness of the method for random-noise attenuation on a 2D earth model. (a) The same synthetic section as in Figure 5b with 10% white-noise addition; (b) output seismograms from K-L filter; (c) output seismograms from *f-x* prediction filter; (d) output seismograms obtained from CTT method.

reflective horizon located at about 1.3 s. Figure 9b shows the result of the application of CTT method to the seismic data for T_w equal to 275 ms. The low-amplitude noise is diminished, and the section has a more simplified appearance; however, the amplitudes of some of the weak reflection events are also reduced. We also observe that most of the amplitude reduction occurs in the deeper parts of the section, while the amplitudes of the shallower reflections are better preserved in the output. Indeed, the CTT algorithm has a stronger filtering effect on the events reflected from deep targets that have experienced a relatively larger loss of high frequencies because of absorption; therefore, the amplitude reduction is larger in the deeper reflections because the CTT algorithm attempts to reduce the amplitudes of low-frequency components of the envelope trace.

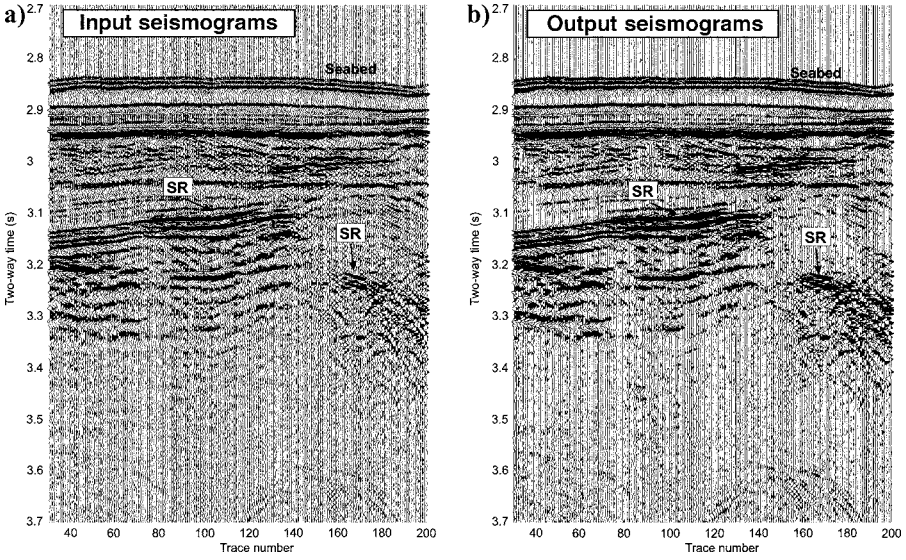

Figure 8. (a) Part of a single-fold common-offset section from northern Black Sea with two strong reflections (bright-spots) indicated as SR; (b) result of application of the method to the section in (a) using T_w equal to 450 ms.

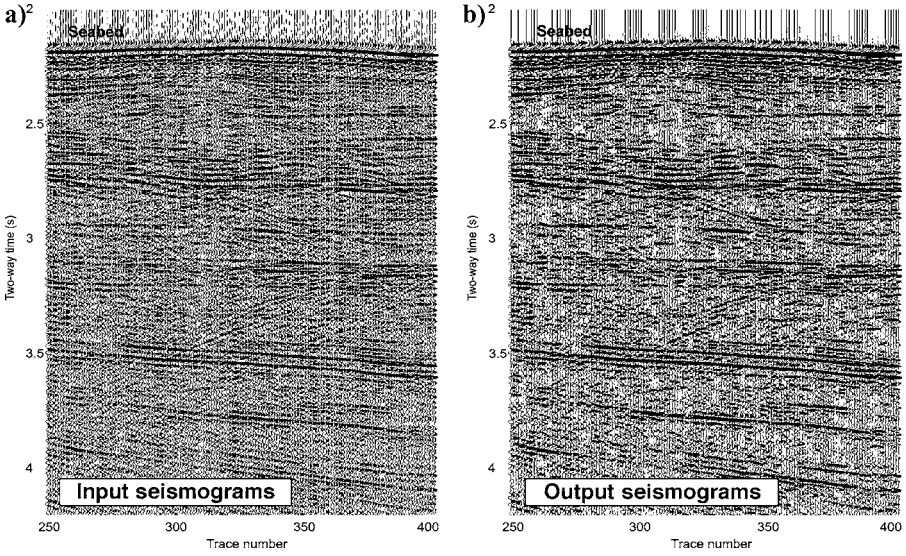

Figure 9. (a) Part of a low-fold seismic line from northern Gulf of Mexico showing a number of parallel and undisturbed sedimentary layers; (b) result of application of the method to the section in (a) using T_w equal to 275 ms.

CONCLUSIONS

Complex-trace transformation is used for temporal resolution improvement and random-noise suppression for stacked seismic data. The method includes omission of the low-frequency component of the amplitude envelope of the stacked trace and calculation of a new trace using normalized phase information.

The primary value of the CTT is that it has the ability to simultaneously reduce random noise and broaden seismic bandwidth. These two objectives are usually in conflict in linear seismic processing. Another advantage of the CTT method is its simplicity. It also does not require much mathematical computation, and the only parameter selection required is T_w. We concluded that the time window length is an important parameter for complex-trace transformation processes, and our tests show that it controls both the noise reduction level and bandwidth (or frequency content) of the output. Both random-noise suppression and temporal-resolution improvement is better for T_w values between $(N/4)\Delta t$ and $(N/8)\Delta t$. For the T_w values outside of this range, the CTT method causes severe main-lobe reduction and temporal resolution improvement becomes also small.

Although complex-trace transformation can also be used on the prestack seismic data, we suggest that it is more convenient to use on stacked data because the stack itself is a powerful technique to reduce the random noise. Therefore, the complex-trace transformation method can be used to reduce remaining noise components and produce further temporal resolution improvement on the poststack data as a secondary tool in conventional seismic processing. It can be successfully used for single channel and low-fold marine seismic data where it is not possible to suppress the random noise by vertical summing and/or multifold CDP stacking. We also suggest the method may be beneficial when used in conjunction with automatic interpretation tools such as automatic event tracking.

ACKNOWLEDGMENTS

We sincerely thank Patrick E. Hart from the United States Geological Survey, Coastal and Marine Geology Group for his valuable and constructive comments on the earlier version of this manuscript. We also wish to thank Herve Nouze from IFREMER, France for his helpful comments especially on the applications of the method. We thank Oleg Krylov from Moscow State University, who kindly supplied the Sorokhin Trough seismic data. The 2D synthetic seismic sections were produced using ray tracing

seismic modeling software OUTRIDER of Digi-Rule Inc. The computations were performed on the workstation supplied by HERMES project, funded by the European Commission. This research is partially supported by a grant (project code 100Y078) from the Scientific and Technical Research Council of Turkey (TUBITAK).

References

Çifçi, G., D. Dondurur, O. Krylov, and M. Ergün, 2003, Application of the complex trace attribute analysis to the seismic data from Sorokhin Trough (Northern Black Sea): 14th International Petroleum and Natural Gas Congress and Exhibition of Turkey.

Farnbach, J. S., 1975, The complex envelope in seismic signal analysis: Bulletin of the Seismological Society of America, **65**, 951–962.

Felsen, L. B., and N. Markuvitz, 1973, Radiation and scattering of waves: Prentice-Hall, Inc.

Gelchinsky, B. Y., and N. A. Karaev, 1980, Heterogeneous seismic models formed by inclusions and investigation of wavefields in them: Annales Geophysicae, **36**, 519–535.

Gelchinsky, B. Y., E. Landa, and V. Shtivelman, 1985, Algorithms of phase and group correlation: Geophysics, **50**, 596–608.

Gülünay, N., 2000, Noncausal spatial prediction filtering for random noise reduction on 3D poststack data: Geophysics, **65**, 1641–1653.

Hart, P. E., A. K. Cooper, D. Twichell, M. Lee, and W. Agena, 1999, High-resolution multichannel seismic-reflection data acquired in the Northern Gulf of Mexico, 1998–99: U. S. Geological Survey, Open-File Report 02-368.

Hemon, C. H., and D. Mace, 1978, The use of the Karhunen-Loeve transformation in seismic data processing: Geophysical Prospecting, **26**, 600–626.

Hornbostel, S., 1991, Spatial prediction filtering in the *t-x* and *f-x* domains: Geophysics, **56**, 2019–2026.

Karsli, H., 2002, Evaluation of stacked seismic traces with complex trace analysis in terms of resolution: Earth Sciences, **26**, 15–26.

Klemperer, S. L., 1987, Seismic noise-reduction techniques for use with vertical stacking: An empirical comparison: Geophysics, **52**, 322–334.

Lee, M. W., P. E. Hart, and W. F. Agena, 2001, Processing strategy for water-gun seismic data from the Gulf of Mexico: U. S. Geological Survey Bulletin 2181.

Morozov, I. B., and S. B. Smithson, 1996, Instantaneous polarization attributes and directional filtering: Geophysics, **61**, 872–881.

Ristau, J. P., and W. M. Moon, 2001, Adaptive filtering of random noise in 2-D geophysical data: Geophysics, **66**, 342–349.

Shtivelman, V., E. Landa, and B. Gelchinsky, 1986, Phase and group time sections and possibilities for their use in seismic interpretation of complex media: Geophysical Prospecting, **34**, 508–536.

Taner, M. T., F. Koehler, and R. E. Sheriff, 1979, Complex seismic trace analysis: Geophysics, **44**, 1041–1063.

Yilmaz, Ö., 1987, Seismic data processing: SEG.